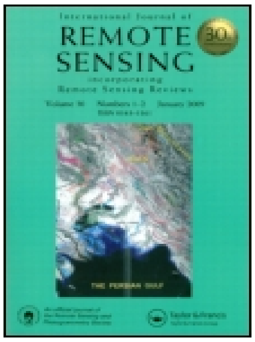

Taylor & Francis
Taylor & Francis Group

International Journal of Remote Sensing

ISSN: 0143-1161 (Print) 1366-5901 (Online) Journal homepage: https://www.tandfonline.com/loi/tres20

Improvement in air–sea flux estimates derived from satellite observations

Abderrahim Bentamy , Semyon A. Grodsky , Kristina Katsaros , Alberto M. Mestas-Nuñez , Bruno Blanke & Fabien Desbiolles

To cite this article: Abderrahim Bentamy , Semyon A. Grodsky , Kristina Katsaros , Alberto M. Mestas-Nuñez , Bruno Blanke & Fabien Desbiolles (2013) Improvement in air–sea flux estimates derived from satellite observations, International Journal of Remote Sensing, 34:14, 5243-5261, DOI: 10.1080/01431161.2013.787502

To link to this article: https://doi.org/10.1080/01431161.2013.787502

International Journal of Remote Sensing, 2013
Vol. 34, No. 14, 5243–5261, http://dx.doi.org/10.1080/01431161.2013.787502

Taylor & Francis
Taylor & Francis Group

Improvement in air–sea flux estimates derived from satellite observations

Abderrahim Bentamy[a]*, Semyon A. Grodsky[b], Kristina Katsaros[c], Alberto M. Mestas-Nuñez[d], Bruno Blanke[e], and Fabien Desbiolles[a,e]

[a]*Laboratoire d'Océanographie Spatiale (LOS), Institut Français pour la Recheche et l'Exploitation de la Mer (IFREMER), France;* [b]*Department of Atmospheric and Oceanic Science, University of Maryland, College Park, MD, USA;* [c]*Rosenstiel School of Marine and Atmospheric Science, University of Miami, Miami, FL, USA;* [d]*Department of Physical and Environmental Sciences, Texas A&M University-Corpus Christi, Corpus Christi, TX, USA;* [e]*Laboratoire de la Physique des Océans (LPO), UMR 6523 CNRS-Ifremer-IRD-UBO, France*

(*Received 15 June 2012; accepted 21 November 2012*)

A new method is developed to estimate daily turbulent air–sea fluxes over the global ocean on a 0.25° grid. The required surface wind speed (w_{10}) and specific air humidity (q_{10}) at 10 m height are both estimated from remotely sensed measurements. w_{10} is obtained from the SeaWinds scatterometer on board the QuikSCAT satellite. A new empirical model relating brightness temperatures (T_b) from the Special Sensor Microwave Imager (SSM/I) and q_{10} is developed. It is an extension of the author's previous q_{10} model. In addition to T_b, the empirical model includes sea surface temperature (SST) and air–sea temperature difference data. The calibration of the new empirical q_{10} model utilizes q_{10} from the latest version of the National Oceanography Centre air–sea interaction gridded data set (NOCS2.0). Compared with mooring data, the new satellite q_{10} exhibits better statistical results than previous estimates. For instance, the bias, the root mean square (RMS), and the correlation coefficient values estimated from comparisons between satellite and moorings in the northeast Atlantic and the Mediterranean Sea are –0.04 g kg^{-1}, 0.87 g kg^{-1}, and 0.95, respectively. The new satellite q_{10} is used in combination with the newly reprocessed QuikSCAT V3, the latest version of SST analyses provided by the National Climatic Data Center (NCDC), and 10 m air temperature estimated from the European Centre for Medium-Range Weather Forecasts (ECMWF) reanalyses (ERA-Interim), to determine three daily gridded turbulent quantities at 0.25° spatial resolution: surface wind stress, latent heat flux (LHF), and sensible heat flux (SHF). Validation of the resulting fields is performed through a comprehensive comparison with daily, *in situ* values of LHF and SHF from buoys. In the northeast Atlantic basin, the satellite-derived daily LHF has bias, RMS, and correlation of 5 W m^{-2}, 27 W m^{-2}, and 0.89, respectively. For SHF, the statistical parameters are –2 W m^{-2}, 10 W m^{-2}, and 0.94, respectively. At global scale, the new satellite LHF and SHF are compared to NOCS2.0 daily estimates. Both daily fluxes exhibit similar spatial and seasonal variability. The main departures are found at latitudes south of 40° S, where satellite latent and sensible heat fluxes are generally larger.

*Corresponding author. Email: abderrahim.bentamy@ifremer.fr

1. Introduction

Accurate turbulent air–sea fluxes (i.e. momentum, latent heat, and sensible heat) are of great interest in regard to a wide variety of air–sea interaction issues. The main sources of such fluxes over the global ocean are numerical weather prediction (NWP) models, voluntary observing ships (VOSs), and remotely sensed data.

For over a decade, several scientific groups have been developing direct and inverse methods, algorithms, and procedures to calculate long time series of surface winds, wind stress, specific air humidity, and latent and sensible heat fluxes; representative data sets include the Japanese Ocean Flux data sets with the Use of Remote sensing Observations (J-OFURO) (Kubota et al. 2002), the Goddard Satellite-based Surface Turbulent Fluxes (GSSTF) (Chou et al. 2003), the Objectively Analysed Air–Sea Fluxes (OAFLUX) (Yu, Weller, and Sun 2004), the Institut Français pour la Recherche et l'Exploitation de la Mer (IFREMER) (Bentamy et al. 2003, 2008), and the Hamburg Ocean Atmosphere Parameters and Fluxes from Satellite Data (HOAPS) (Anderson et al. 2010). These satellite fluxes are widely used by the scientific community for various purposes such as forcing ocean circulation models (e.g. Ayina et al. 2006), studying the spatial and temporal variability associated with the El Niño Southern Oscillation (ENSO) (e.g. Mestas-Nuñez, Bentamy, and Kristina 2006), or employing an enhanced spatial and temporal sampling provided by remote techniques to evaluate intra-seasonal variability (e.g. Grodsky et al. 2009). Even though the results of these investigations have increased our understanding of air–sea interactions, further improvements of satellite-based fluxes are still required.

A number of studies assessing the quality of turbulent fluxes have been published in recent years. By comparing latent heat fluxes (LHFs) from buoys and satellites, Bourras (2006) has found that the overall accuracy is of the order of 20–30%, whereas the required error for a quantitative use over the global oceans should be lower than 10%. He has concluded that the main LHF error sources are related to the accuracy of the specific air humidity (q) and surface wind speed (w). Tomita and Kubota (2006) have investigated the accuracy of satellite-based LHF through comparisons with buoy and NWP estimates. In the tropics, the main source of buoy and satellite LHF discrepancy is attributed to the accuracy of satellite q, whereas around Japan the LHF discrepancy is associated with the accuracy of both w and q. They both have concluded that the improvement in satellite LHF estimation requires improvements in remotely sensed w and q at global and regional scales. Santorelli et al. (2011) have conducted detailed investigations on the accuracy of IFREMER and OAFLUX latent and sensible heat fluxes, as well as of basic bulk variables (10 m wind speed, w_{10}; 10 m specific air humidity, q_{10}; 10 m air temperature, t_{10}; and SST) using standard moored buoy and scientific data from dedicated experiments. Their conclusions generally agree with the studies mentioned earlier. In particular, they emphasized that improvement in satellite fluxes should include improvement in the interpolation method used to calculate gridded fields over the global ocean to better reflect conditions during synoptic-scale storms and fronts.

Following the suggested recommendations for improving fluxes, the present study aims to enhance the following three aspects: the determination of q_{10} retrievals over the global oceans, the accuracy of bulk variables and associated turbulent fluxes, and the spatial and temporal resolutions of the flux fields. This study takes advantage of the availability of new air–sea interaction data sets estimated from the updated International Comprehensive Ocean–Atmosphere Data Set (ICOADS) (Berry and Kent 2011), and of the new QuikSCAT wind retrievals (Fore et al. 2011).

The statistical parameters defined by Bentamy, Katsaros, and Queffeulou (2011), aiming to characterize differences between *in situ* and satellite data, are used to assess the quality of satellite bulk variables and fluxes.

2. Data

The main basic bulk variables required for turbulent flux estimations are surface wind speed (w), specific air humidity (q), specific surface humidity (s), air temperature (t), and sea surface temperature (SST). Moored buoys, ships, and NWP models provide valuable estimates of these variables with various spatial and temporal resolutions. They are used in this study for the calibration and/or validation of satellite retrievals at local, regional, and global scales.

2.1. Scatterometer data

To ensure homogeneity of w and its variability, this study employs only wind retrievals from the SeaWinds scatterometer on board QuikSCAT. The QuikSCAT scatterometer is described in many scientific papers; readers may find a complete description in JPL (2006), including instrument physics, retrieval and ambiguity removal methods, rain detection and flagging techniques, and quality control procedures. Briefly, QuikSCAT is a rotating antenna with two emitters of different polarity: H-pol with an incidence angle of 46.25° and V-pol with an incidence angle of 54°. The inner beam has a swath width of about 1400 km, while the outer beam swath is 1800 km in width. Since the QuikSCAT scatterometer is a Ku-band radar, rain has a substantial influence on its measurements. Previous studies showed that the rain impact may attenuate the scatterometer signal resulting in wind speed underestimation, or raindrop impacts may change the sea surface shape resulting in overestimation of the retrieved winds. Results from Portabella et al. (2012) indicate that rain backscatter contributes to the scatterometer signal, resulting generally in wind speed overestimation; intense rain causes overestimates of 15–20 m s^{-1} for cross-track winds. So, rain attenuation dominates over rain backscatter in regard to extreme winds. QuikSCAT wind products include several rain flags determined from the scatterometer's observations and from the collocated radiometer rain rate on board other satellites.

This study uses QuikSCATV3, the latest version of QuickSCAT wind retrievals (ftp://podaac.jpl.nasa.gov/OceanWinds/quikscat/preview/L2B12/v3/). They have been made available by the Jet Propulsion Laboratory (JPL)/Physical Oceanography Distributed Active Archive Center (PODAAC) scientific team (Fore et al. 2011). QuikSCAT V3 products are calculated through use of a geophysical model function ensuring consistency with winds retrieved from microwave radiometers such as the Special Sensor Microwave Imager (SSM/I) and WindSat (Ricciardulli and Wentz 2011). QuickSCAT wind retrievals are provided over swaths at a wind vector cell (WVC) of 12.5 km spatial resolution. This new scatterometer product is assumed to improve wind speed performance in rain and at high wind speeds.

The accuracy of QuikSCATV3 data is determined through various comparisons with buoy wind measurements, QuikSCATV2 retrievals, and remotely sensed winds derived from the C-band, ASCAT scatterometer aboard the Metop-A satellite. The main findings (not shown) are the results of the comparisons and are similar to those obtained previously (Bentamy et al. 2012). QuikSCATV3 and QuikSCATV2 exhibit similar comparison results versus buoys. ASCAT and QuikSCATV3 statistics are of the same order as ASCAT and QuikSCATV2. Similar discrepancies characterizing ASCAT and QuikSCATV2 comparisons are found for ASCAT and QuikSCATV3. For instance, the most significant discrepancies are found at tropical and high latitudes. QuikSCATV3 are improved when compared with the earlier results reported by Bentamy et al. (2012). We expect that the remaining discrepancies between C-band radar and Ku-band radar wind retrievals are inherent in their characteristics, including the radar's penetrating wavelengths and backscatter interactions with surface waves at different wavelengths. Such effects would be pronounced in low wind speed regimes and at certain values of SST.

2.2. Radiometer data

The SSM/I measurements used in this study are the same as those in Bentamy et al. (2003, 2008). The SSM/I radiometers on board the Defense Meteorological Satellite Program (DMSP) F11, F13, F14, and F15 satellites provide measurements of surface brightness temperatures (T_b) at frequencies 19.35, 22.235, 37, and 85 GHz (hereafter referred to as 19, 22, 37, and 85 GHz), respectively. Horizontal and vertical polarization measurements are taken at 19, 37, and 85 GHz. Only vertical polarization is available at 22 GHz. Owing to the choice of channels operating at frequencies outside strong absorption lines (for water vapour 50–70 GHz), the detected radiation is a mixture of radiation emitted by clouds, water vapour in the air, and the sea surface, as well as radiation emitted by the atmosphere and reflected at the sea surface. Brightness temperature measurements as well as the associated geophysical parameters are provided by the Global Hydrology Resource Center (GHRC) (http://ghrc.msfc.nasa.gov/).

2.3. Buoys

Data from a number of moored buoys located in different basins are used for ground truth validation. These include eight Atlantic moorings off the French and English coasts, maintained by the UK Met Office and/or Météo-France (MFUK), 96 moorings off the Atlantic and Pacific US coasts, maintained by the US National Data Buoy Center (NDBC), 66 moorings of the Tropical Atmosphere Ocean (TAO) array in the equatorial Pacific, 13 moorings of the Prediction and Research Moored Array in the Atlantic (PIRATA) network in the equatorial Atlantic, and 9 moorings of the Research Moored Array for African-Asian-Australian Monsoon Analysis and Prediction (RAMA) project. TAO, PIRATA, and RAMA will be hereafter referred to as tropical buoys. Meteorological buoy data are provided as hourly averages. Measurement height varies between 3 and 10 m depending on mooring configuration. Buoy wind, specific air humidity, and air temperature are converted to the standard height of 10 m using the COARE3.0 algorithm of Fairall et al. (2003). The latter is also used to estimate buoy turbulent fluxes.

2.4. NOCS data

A new daily mean air–sea interaction gridded data set (Berry and Kent 2011) is provided by the National Oceanography Centre, Southampton, and is referred to as the NOCS Flux Data set v2.0 (NOCS2.0). The gridded values are available over the global ocean with a spatial resolution of $1° \times 1°$. Daily parameters such as w_{10}, q_{10}, t_{10}, SST, LHF, and SHF are provided with uncertainty estimates. The accuracy of NOCS2.0 gridded parameters was investigated through various comparisons including buoy, satellite, and numerical model data. For instance, comparison with buoys deployed and maintained by the Woods Hole Oceanographic Institution (WHOI) Upper Ocean Processes Group (UOP) indicates that the mean differences (NOCS2.0–WHOIUOP) of w_{10} and q_{10} are about 0.30 m s^{-1} and 0.40 g kg^{-1}, respectively (Table II of Berry and Kent 2011).

2.5. ERA-Interim

ERA-Interim (Simmons et al. 2006) refers to the reanalyses of atmospheric parameters produced by the European Centre for Medium-Range Weather Forecasts (ECMWF). It uses

4D-variational analysis on a spectral grid and covers 1989 to the present. The ERA-Interim data used in this study were obtained from the ECMWF data server on a fixed grid of 0.75°. The main parameters used in this study are specific air humidity and air temperature at 2 m, available at synoptic times (00:00:00, 06:00:00, 12:00:00, 18:00:00 UTC), which are converted to q_{10} and t_{10}, respectively, utilizing the COARE3.0 model (Fairall et al. 2003). The quality of q_{10} and t_{10} is checked through comparisons with MFUK, TAO, and PIRATA buoy estimates. The main finding of interest for this study is that ERA-Interim t_{10} is underestimated for buoy t_{10} exceeding 20°C. A bias correction is determined from linear regression between ERA-Interim and buoy t_{10} estimates.

2.6. Collocation

For q_{10} calibration purposes, values of q_{10} and SST from the SSM/I, NOCS2.0, and ERA-Interim are collocated in space and time. SST data are from version 2 of the optimum interpolated (OI) daily SST analyses (Reynolds et al. 2007) with a spatial resolution of 0.25°. A common collocation procedure is utilized. ERA-Interim q_{10} and t_{10} occurring within 50 km and three hours of a SSM/I cell location and time, respectively, are bi-linearly interpolated in both space and time at the SSM/I cell. SSM/I brightness temperatures and NOCS2.0 q_{10} occurring on the same day are matched if the spatial difference is less than 100 km. The same collocation approach is used for SSM/I T_b and daily SST, except that the spatial difference criterion is 25 km.

3. Specific air humidity improvement

3.1. Retrieving specific air humidity from satellite measurements

Based on collocated SSM/I and ICOADS data, several authors have assessed the relationship between satellite brightness temperature (T_b) and *in situ* specific air temperature (e.g. Kubota et al. 2008; Jackson, Wick, and Robertson 2009). The former is mainly related to the linear relationship between specific air humidity and column integrated water vapour content (v) obtained from satellite microwave radiometers (Schulz, Schlussel, and Grassl 1993). SSM/I T_b measurements are sensitive to v especially in the 19V, 19H, 22V, and 37V channels. In Bentamy et al. (2003), the development of a SSM/I-based method for the retrieval of q_{10} from brightness temperatures is based on a model determined from collocated SSM/I T_b and COADS q_{10} over limited oceanic areas of the North Atlantic and eastern equatorial Pacific, and during a limited period (1996–1998). This model was successfully used by several groups for q_{10} estimation from either SSM/I or AMSRE measurements, as well as to assess the development of new q_{10} models (e.g. Anderson et al. 2010; Kubota et al. 2008; Jackson, Wick, and Robertson 2009). However, Grodsky et al. (2009) and Santorelli et al. (2011) underlined the need for improvement in remotely sensed specific air humidity. To achieve such enhancement, the newly updated and enhanced NOCS2.0 data are used as references for new q_{10} modelling. For instance, Figure 1 shows the difference between NOCS2.0 and the previous version of satellite q_{10} of Bentamy et al. (2003) as a function of satellite-derived q_{10} and for five NOCS2.0 SST ranges. The findings (Figure 1) suggest inclusion of SST as a variable in a satellite q_{10} model. Furthermore, investigation of NOCS2.0 and satellite q_{10} differences indicates a stratification dependency. The latter would be an indication of the modification of the relationship between v and q as a function of stratification variability. Therefore, the new q_{10} model includes terms related to SST and to differences between 10 m air and SSTs (ΔT):

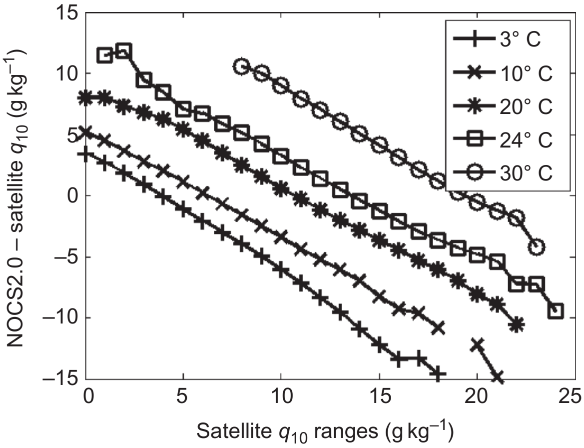

Figure 1. NOCS2.0 minus satellite q_{10} difference as a function of satellite q_{10}. Lines are average difference in 1 g kg^{-1} satellite q_{10} bin for data grouped in the five SST bins. Satellite (IFREMER) q_{10} is from Bentamy et al. (2003).

$$q_{10} = f_1\left(T_{\mathrm{b},19\mathrm{V}}\right) + f_2\left(T_{\mathrm{b},19\mathrm{H}}\right) + f_3\left(T_{\mathrm{b},22\mathrm{V}}\right) + f_4\left(T_{\mathrm{b},37\mathrm{V}}\right) + g(\mathrm{SST}) + h(\Delta T). \quad (1)$$

The functions f_1, f_2, f_3, f_4, g, and h are determined through a maximum likelihood procedure based on the use of collocated data: SSM/I F11T_b, NOCS2.0 q_{10}, SST, and ERA-Interim t_{10}. Only matchups occurring during January, April, August, and September 2005 are used for q_{10} model calibration, thus leaving the remaining *in situ* data for verification purposes. Owing to the strong correlation between v and brightness temperatures, and the correlation between specific air humidity and SST, q_{10} in Equation (1) is mainly weighted by functions f_1,f_2,f_3,f_4, h, and g. Overall, although the term $h(\Delta T)$ has a small impact, it maintains the bias between NOCS2.0 and satellite q_{10} close to zero with respect to the air–sea temperature difference.

3.2. Daily analysis

This study aims at estimating daily 10 m specific air humidity from radiometer retrievals. However, one should assess the meaning of daily averaged q_{10} based on the use of limited remotely sensed observations. Indeed, local equator crossing times of the SSM/I at the ascending node are about 19 hours for F11, 18 hours for F13, 20 hours (1999) and 17 hours (2009) for F14, and 21 hours (2000) and 18 hours (2009) for F15. Such radiometer orbit characteristics lead to limited observations during morning and evening local times. The impact of the radiometer sampling scheme on the accuracy of the calculation of q_{10} daily estimates is evaluated using hourly buoy q_{10} data. For each buoy, two kinds of daily averaged estimates are calculated. The first $(\overline{q_a^b})$ is determined as an arithmetic mean of all available daily measurements (generally 24-hourly data), whereas the second $(\overline{q_a^s})$ is calculated as an arithmetic mean of hourly buoy q_{10} collocated in space (distance less than 25 km) and time (separation time less than 1 hour) with radiometer passes. Differences between $\overline{q_a^b}$ and $\overline{q_a^s}$ are investigated based on the use of MFUK and tropical buoy q_{10} measurements (figures not shown). In the Eastern Atlantic and Mediterranean Sea, $\overline{q_a^b}$ and $\overline{q_a^s}$ differences, estimated at each buoy location, exhibit a similar behaviour. The mean differences are low (0.18 g kg^{-1}), indicating that $\overline{q_a^s}$ are slightly underestimated when compared with $\overline{q_a^b}$. The associated root mean square (RMS) values are lower than 0.40 g kg^{-1}. In the tropical basins, where specific air humidity values are maximal, the mean differences are close to zero, and RMS values do not exceed 0.40 g kg^{-1}. The results characterizing $\overline{q_a^b}$ and $\overline{q_a^s}$ differences do not exhibit any significant geophysical patterns, except at a buoy located off the coast of the Mediterranean Sea. Therefore, we conclude that daily average air humidity based on the particular temporal sampling of satellite observations deviates from the 'true' daily mean by less than 0.18 g kg^{-1}. The magnitude of this bias is considered as the characteristic error of satellite q_{10}, as can be seen below.

These results allow the determination of daily averaged 10 m specific air humidity from radiometer brightness temperature measurements. They are estimated as gridded fields with the same spatial resolution as the gridded daily wind fields (see the following section). All available and valid brightness temperature measurements from F11, F13, F14, and F15 satellites during 2005–2007 are used. For each day and for each individual SSM/I swath cell, valid brightness temperatures (instantaneous) and the spatially closest daily averaged SST and 6-hourly 10 m air temperature are selected. Specific air humidity is estimated based on Equation (1). Time differences and accuracy characteristics (Meissner, Smith, and Wentz 2001) of brightness temperatures derived from various instruments may contribute to an inconsistency between q_{10} derived from Equation (1) and actual values expected to be used for the daily gridded specific air humidity calculation. To reduce the non-consistency impact, auxiliary information providing a mean description of q_{10} during a given day is also used. It is derived from 6-hourly ERA-Interim q_{10} estimates (q_{mod}). The following linear relationship between retrievals (q_{10}) and auxiliary data q_{mod} is assumed:

$$E(q_{10}\,(x,y,t)) = \alpha_0 + \beta_1 q_{\text{mod}}\,(x,y,t)\,, \tag{2}$$

where x, y, and t represent spatial and temporal coordinates, and α_0 and β_1 are coefficients to be estimated. The operator E is the mathematical mean (conventional first moment), and q_{mod} indicates Era-Interim q_{10} collocated in space and time with each individual satellite retrieval. Equation (2) is known as the external drift constraint (Wackernagel 1998).

The objective method aiming to calculate gridded daily specific air humidity from retrievals is similar to the method used for daily ASCAT wind field analyses (Bentamy and Croizé-Fillon 2011). Daily satellite q_{10} (q_{sat}) is estimated based on the following assumption:

$$q_{\text{sat}} = \frac{1}{(t_{\text{b}} - t_{\text{a}})} \int_{t_{\text{a}}}^{t_{\text{b}}} \left(\sum_{j=1}^{N} \lambda_j (q_{10}(x_j, y_j, t) \right) \mathrm{d}t + \varepsilon, \tag{3}$$

with unbiased constraint $\sum_{j=1}^{j=N} \lambda_j = 1$ and external drift constraint (Equation (2)), where q_{10} (x_j, y_j, t) indicates the jth q_{10} retrieval available over a given satellite swath cell with geographical coordinates (x_j, y_j) and at time t. t_{a} and t_{b} indicate the time interval falling between 00:00:00 and 23:59:59 (UTC) when retrievals are available. N is the retrieval number selected for daily analysis calculation; $\boldsymbol{\lambda}$ is the weighting vector to be estimated and is the solution of the following linear system:

$$\sum_{j=1}^{j=N} \lambda_j C_{ij} - \mu_1 - \mu_2 q_{\text{modi}} = C_{i0} \quad \text{for } i = 1, 2, 3, \ldots, N$$

$$\sum_{j=1}^{j=N} \lambda_j = 1 \tag{4}$$

$$\sum_{j=1}^{j=N} \lambda_j q_{\text{mod},j} = q_{\text{mod},0},$$

where $\mathbf{C}_{ij}$ stands for the covariance matrix between q_{10} observations, while μ_1 and μ_2 are the Lagrangian terms used to take into account the unbiased and external drift constraints. Index 0 indicates the grid point where daily analysis is performed.

The objective method requires parameterization of the spatial and temporal covariance structure of specific air humidity. It is determined from retrievals occurring during January, April, July, and October 2005 over the global ocean between 55° S and 55° N.

3.3. Accuracy of satellite daily specific air humidity

The quality of the resulting daily satellite q_{10} estimates (q_{sat}) is mainly investigated through comprehensive comparisons with daily averaged 10 m specific air humidity (q_{buoy}) from buoys during 2005–2007, for which period both new (q_{sat}) and old ($q_{\text{sat\_old}}$) values are available. Daily buoy estimates are calculated as an arithmetic mean of all valid hourly data. For each day within the period, all daily buoy and satellite data separated by less than 25 km are selected. Consequently, 2910 collocations from MFUK and 16,999 from tropical networks, with specific air humidity ranging from 2 to 25 g kg^{-1}, met all the collocation quality control criteria. The buoy–satellite comparisons are complemented by comparisons with daily ship data from NOCS2.0 for two regions: a low-humidity region in the mid-latitude North Atlantic and Mediterranean Sea (20° W–10° E, 35° N–60° N) and a more humid region in the tropical Atlantic (70° W–10° E, 15° S–15° N). These regions are selected based on ground truth mooring locations. The northern region hosts the MFUK moorings while the tropical region hosts the PIRATA mooring array. In addition, the quality of the daily satellite q_{10} analysis is investigated on global scales through comparisons with daily estimates from NOCS2.0 and ERA-Interim. Only the 2007NOCS2.0 q_{10} are used for the global comparisons because these data were excluded from the calibration of the q_{10} model (1).

Even though buoy as well as ship q_{10} data are used as ground truth references, both sources may have uncertainties mainly related to hygrometer type, measurement height, and solar radiation contamination (Kent, Woodruff, and Berry 2007). The assessment of the quality of the reference data is beyond the scope of this article.

To limit possible impacts of sampling errors of *in situ* data, comparisons are limited to q_{10} with relative random error less than 10%. Most of the cases (>95%) when this error exceeds 10% occur in dry conditions ($q_{10} < 4$ g kg^{-1}) at the MFUK buoys. The statistics established for these specific cases yield an overestimation of satellite q_{10}.

Figures 2(*a*) and (*b*) illustrate validation results obtained for MFUK and tropical moorings, respectively. The statistics characterizing buoy and satellite comparisons are estimated. Table 1 provides the biases and standard deviations (STDs) of buoy and satellite differences (in that order), and correlation coefficients (*r*). The statistics associated with the performance of daily q from Bentamy et al. (2003) indicated as $q_{\text{sat\_old}}$ are also provided. The updated daily satellite q_{sat} gives a good representation of daily *in situ* q_{10} estimates. Correlation coefficients between tropical and satellite and between MFUK and satellite daily q_{10} are 0.85 and 0.95, respectively. At MFUK buoy locations, correlation

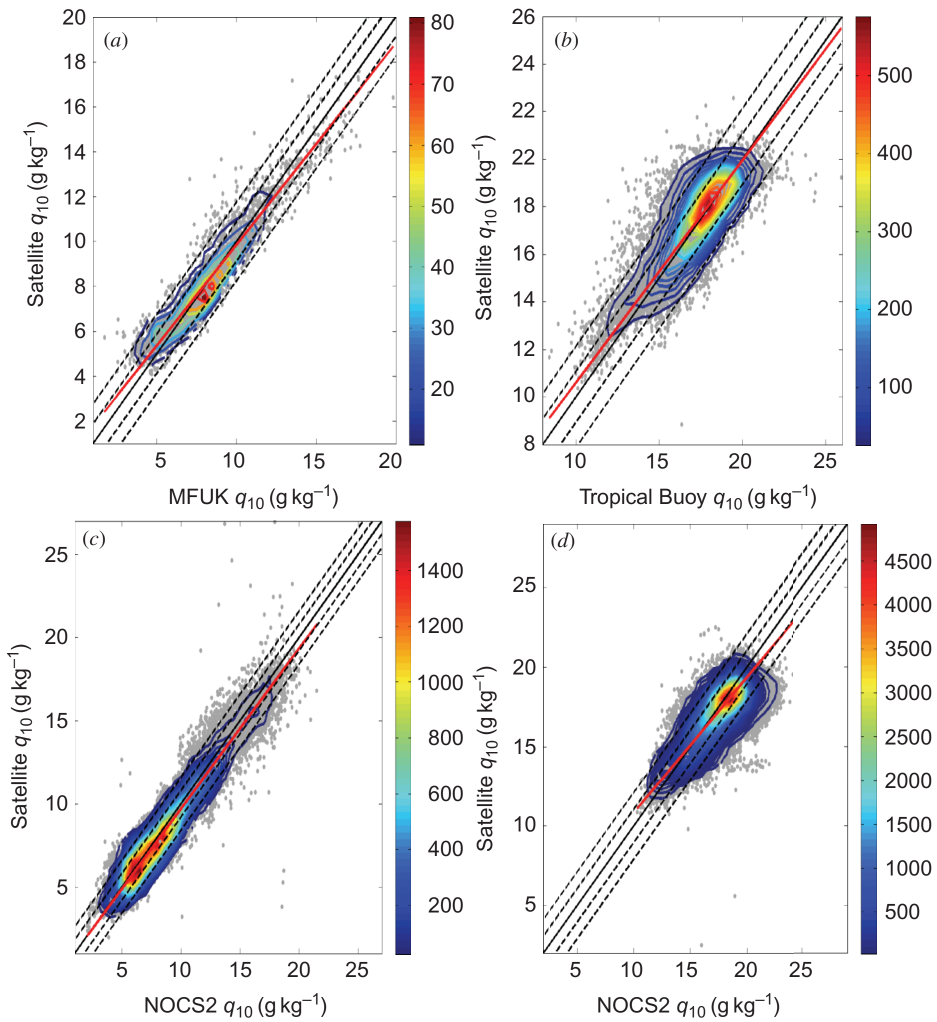

Figure 2. Daily averaged specific air humidity from buoys (MFUK (*a*) and tropical (*b*)) and satellites. Panels (*c*) and (*d*) show companion comparisons with daily NOCS2.0 q_{10} from the two areas surrounding MFUK and tropical arrays, respectively. Black and red lines are perfect and symmetrical linear fits, respectively. Inner and outer dashed lines show one and two standard deviations of *in situ* minus satellite q_{10}, respectively. Numbers in the colour bars represent the number of collocated data per 0.50 g kg^{-1} bins. Only bins with the number of collocated data exceeding a threshold (30 for mooring and 100 for NOCS2.0 comparisons) are shown in colour. The rest of the collocated data are shown as grey dots.

coefficient varies between 0.92 and 0.95 leading to no significant location dependence. Even though correlation coefficients are quite high at tropical locations, better results are found at buoys moored off the Equator, where polar-orbiting satellite sampling is better than at low latitudes. NOCS2.0 and satellite q comparisons (Table 1) indicate similar correlation results.

The biases for the new q_{10} are low (Table 1) and are not statistically significant. Biases increase for low and high q_{10} (Figures 2(*a*) and (*b*)), indicating slight overestimation and underestimation, respectively, which is also evident from the regression fit lines in Figure 2.

Table 1. Statistical parameters of differences between daily buoys (MFUK, TAO, PIRATA, RAMA) and satellite specific air humidity estimated for 2005–2007. Bias, STD, and *r* stand for mean and standard deviation difference (buoy minus satellite) values, and correlation coefficients, respectively. Bias and STD are in g kg^{-1} units.

		q_{sat}			q_{sat_old}		
	Length	Bias	STD	*r*	Bias	STD	*r*
MFUK	2910	−0.04	0.87	0.95	−0.20	1.43	0.90
TAO/PIRATA/RAMA	16,999	−0.10	1.05	0.85	0.88	1.62	0.75
NOCS2.0 (MFUK)	67,104	0.23	0.79	0.95	0.42	1.57	0.88
NOCS2.0 (Tropical)	129,341	0.27	1.05	0.83	0.74	1.55	0.73

However, the bias always stays within one STD. Therefore, the bias behaviour as a function of buoy q_{10} ranges may be partly related to the collocation procedures (satellite data coverage and q_{10} latitude dependency), to differences in estimates of daily averaged buoy and satellite q_{10}, and to differences in the buoy and satellite temporal and spatial sampling schemes. The highest departure between daily averaged buoy and satellite q_{10} is depicted in the Pacific warm pool region. Satellite q_{10} tends to be overestimated compared with *in situ* estimates. Furthermore, buoy q_{10} exhibits higher temporal variability than that reported from satellite q_{10}. Similar bias dependencies on q_{10} are present in comparisons with NOCS2.0 q_{10} (Figures 2(*c*) and 2(*d*)). Biases at buoy locations (where at least one year of collocated data are available) display weak geographical variations. Air humidity bias varies from –0.10 to 0.10 g kg^{-1} at the mid-latitude MFUK locations, but the bias range increases in more humid tropical conditions where it varies from –0.30 to 0.30 g kg^{-1} at the tropical mooring locations, except at the 125° W, 2° S TAO mooring where the bias is anomalously strong, reaching 0.90 g kg^{-1}. The bias analysis indicates that the q_{10} model (Equation (1)) works better in extra-tropical areas where most of the water vapour is trapped near the surface and when assessing the relationship between v and q. However, the q_{10} model is less accurate in regions of active convection where water vapour may exist aloft, and this is related to atmospheric processes that are not highly correlated to surface fluxes, especially at a daily scale.

STD of daily satellite and *in situ* (buoy and ship) specific air humidity is also weaker at mid-latitudes and increases in the tropics (Table 1); STD increases from 0.79 to 1.05 g kg^{-1}. It depicts weak changes among buoy locations with the exception of higher values in the Mediterranean Sea, where STD is about 1.10 g kg^{-1}. At the two Mediterranean MFUK locations, atmospheric conditions are strongly variable. For instance, STD of specific air humidity measured by MFUK buoys moored in the Mediterranean Sea is twice as strong as that at the Atlantic MFUK moorings. Better satellite data sampling is needed to decrease STD between satellite and buoy data in the Mediterranean Sea.

The newly developed algorithm used for estimating satellite daily specific air humidity provides significant improvements over the previous example (Bentamy et al. 2003). Indeed, statistics characterizing comparisons between buoy and satellite, as well as NOCS2.0 and satellite, clearly show that results are better for the updated q_{sat} in various study regions (Table 1). For instance, RMS difference values between the new and old daily satellite q_{10} estimates (estimated from bias and STD values) are reduced by more than 50%.

At a global scale, the updated q_{sat} are compared with daily averaged 10 m q from NOCS2.0 (q_{nocs}). The two q_{10} sources are collocated in space and time. For each day, q_{sat} values are linearly interpolated over a q_{mod} gridded map. The resulting collocated daily data are used to estimate monthly, seasonal, and annual statistical parameters, such as mean and STD of each q product, mean and STD differences, and correlation coefficient between q_{nocs} and q_{sat} (in this order). Only results derived from collocated data occurring during 2007 are shown. They are not used for calibration dealing with the determination of the retrieval model (Equation (1)).

The spatial variability of specific air humidity from the two products exhibits very similar features for both monthly and seasonal and annual scales. The former are highly related to spatial patterns of SST and precipitation and the major spatial patterns of specific air humidity (Jackson, Wick, and Robertson 2009). For instance, Figure 3 illustrates q_{sat} spatial patterns estimated for the northern hemisphere (NH) winter (December–January–February, DJF), spring (March–April–May, MAM), summer (June–July–August, JJA), and autumn (September–October–November, SON). q_{10} values exceeding 18 g kg^{-1} are mainly found along the convergence zones in the tropical Atlantic, Pacific, and Indian oceans. High values reaching or exceeding 19 g kg^{-1} are depicted in the western Pacific warm pool throughout the year, in the tropical and northeastern Indian Ocean areas during spring and summer seasons, respectively, and in the Caribbean and Gulf of Mexico during summertime. Seasonal variations result in significant differences in specific air humidity estimates between NH winter and summer. They reach 6 g kg^{-1} in northeastern oceanic regions, north of the Indian Ocean, the Gulf of Mexico, over the entire Mediterranean Sea, off the northwestern African coasts, and over the southeastern Indian Ocean. Such spatial and seasonal patterns are likely closely related to those of SST.

The spatial differences between NOCS2.0 and satellite q_{10} during NH winter and summer seasons are shown in Figure 4. Upper and lower panels illustrate bias and STD differences, respectively. The new q_{sat} daily estimates reduce the discrepancies between *in situ* and satellite in terms of both mean difference and variability. Indeed, previous studies reported that the IFREMER (old version) specific air humidity was underestimated by 1 g kg^{-1} compared with ICOADS over the inter-tropical ocean (Jackson, Wick, and Robertson 2009), while it was slightly overestimated over subtropical oceanic areas. Both statistical parameter spatial distributions (Figure 4) do not exhibit significant geophysical

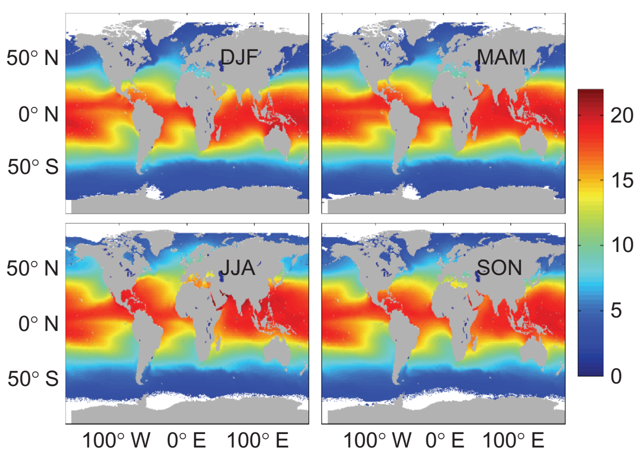

Figure 3. Northern hemisphere winter (December–January–February (DJF)), spring (March–April–May (MAM)), summer (June–July–August (JJA)), and autumn (September–October–November (SON)) mean q_{10} patterns estimated from daily satellite analyses for the period 2005–2007. Colour indicates q_{10} values in g kg^{-1}.

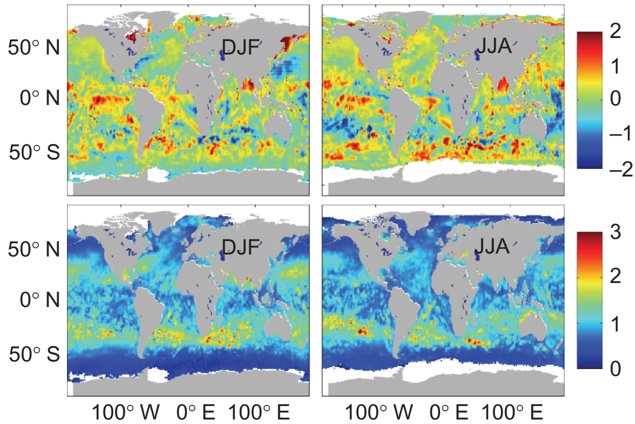

Figure 4. Mean difference (top) and standard deviation (bottom) between daily NOCS2.0 and satellite q_{10} for boreal winter (DJF) and summer (JJA) during 2005–2007. Colour indicates mean and STD values in g kg^{-1}.

pattern dependency. More than 84% (DJF) and 95% (JJA) of q difference values are lower than 1 and 1.5 g kg^{-1}, respectively, whereas the associated STDs are lower than 2 g kg^{-1} for 95% of total grid points. Most of the differences exceeding 1 g kg^{-1} are found in the southern ocean and/or in regions where NOCS2.0 q error exceeding 1.3 g kg^{-1} is associated with issues related to sampling by ships (Berry and Kent 2011). Excluding these poorly sampled regions leads to an improvement in NOCS2.0 and satellite comparisons: more than 95% of differences do not exceed 1.20 g kg^{-1}. At regional scales, two areas located in the northwestern Atlantic and Pacific oceans, likely related to Gulf Stream and Kuroshio currents, are depicted during NH winter season. Specific air humidity is assumed to be low (Figure 4) due to continental cold air outbreaks. These discrepancies might be partly related to the uncertainties of the retrieval model (Equation (1)) at some specific locations and for some local atmospheric and oceanic conditions.

4. Daily wind fields

Surface wind speeds and directions may be retrieved from scatterometers and radiometers. In this study, only QuikSCATV3 retrievals are used. As mentioned in Section 2, these are corrected with respect to the results of Bentamy et al. (2012). The calculation of daily gridded wind fields from scatterometer wind observations is performed using the same objective method as that for the estimation of daily ASCAT wind fields (Bentamy and Croizé-Fillon 2011). The resulting wind field accuracy is investigated through comparison with daily averaged winds from MFUK, NDBC, PIRATA, RAMA, and TAO moored buoy estimates. The main statistics characterizing scatterometer and buoy daily wind speeds and direction comparisons are summarized in Table 2. Bias and STD are mean and STD values of differences between buoy and satellite data, respectively. r is the correlation coefficient, and for wind direction, it is estimated as vector correlation (Bentamy and Croizé-Fillon 2011b). It varies between –2 and +2. The overall statistics indicate that the daily scatterometer wind fields compare well to daily averaged buoy data. RMS differences do not exceed 2 m s^{-1} and 20°, which are the scatterometer specifications for wind speed and direction, respectively. For *in situ* and scatterometer daily winds higher than 3 m s^{-1}, no

Table 2. Statistical parameters of differences between daily buoys (MFUK, NDBC, TAO, PIRATA, RAMA (tropical)) and satellite wind speeds ($m\ s^{-1}$), wind directions (°), wind stress amplitude (dyn m^{-2}), latent heat flux (LHF) ($W\ m^{-2}$), and sensible heat flux (SHF) ($W\ m^{-2}$). Numbers to the right of mooring names are sampling lengths of buoy and satellite-collocated daily data.

	MFUK (12146)			NDBC (28048)			Tropical (49843)		
	Bias	STD	*r*	Bias	STD	*r*	Bias	STD	*r*
Speed	−0.36	1.58	0.92	−0.27	1.09	0.94	−0.25	1.25	0.85
Direction	0.00	19.00	1.76	−5.00	23.00	1.74	−4.00	17.00	1.65
Stress	−0.01	0.07	0.92	−0.01	0.04	0.95	−0.01	0.03	0.85
Latent heat	5.00	27.00	0.89	13.00	37.00	0.89	2.00	31.00	0.79
Sensible heat	−2.00	10.00	0.94	−2.00	10.00	0.96	−4.00	6.00	0.77

significant bias trend is found. For lower wind speed ranges, scatterometer winds tend to be slightly overestimated compared with those estimated by buoys. The biases in wind direction are relatively small. Despite differences in buoy and scatterometer sampling schemes used for the estimation of daily winds, correlation values attest that satellite daily winds reproduce *in situ* estimates fairly well. The lowest correlation value is found for tropical buoy and satellite wind comparisons, due to the low wind speed conditions within these specific oceanic regions.

5. Turbulent fluxes

Daily surface wind stress and the associated zonal and meridional wind stress components, and surface latent and sensible heat fluxes are estimated over global oceans from daily winds (Section 4), specific air humidity (Section 3), SST, and air temperature utilizing the COARE3.0 bulk parameterization algorithm (Fairall et al. 2003). SST are from the daily OI analyses (Reynolds et al. 2007), while t_{10} are daily averaged estimates calculated from Era-Interim analyses (Section 2). Calculations of gridded bulk variables and turbulent flux fields are performed over global oceans with a spatial resolution of 0.25° in both longitude and latitude. Spatial and temporal resolutions of the flux fields are consistent with SST analyses.

The quality of the new flux fields is first examined through comparisons with turbulent fluxes estimated from daily averaged, buoy bulk variables. Most NDBC buoys do not provide measurements of specific air humidity (or relative humidity); these are calculated from air and dew point measurements. Since daily turbulent fluxes are estimated utilizing COARE 3.0 parameterization, any departures between buoy and satellite daily fluxes highlight differences in daily bulk variables. In this article, statistics related to comparisons between buoy and satellite daily wind stress (τ), latent (LHF), and sensible (SHF) heat fluxes are provided (Table 2). These are calculated from collocated buoy and satellite data for 2005–2007.

As expected, buoy and satellite daily wind stress exhibit similar comparison results to those found for wind speed (Table 2). This is clearly illustrated by correlation coefficient values. Furthermore, negative bias values are associated with a slight overestimation of satellite wind speeds.

Daily satellite LHF is slightly underestimated in comparison with buoy data. Biases from the MFUK, NDBC, and tropical moorings are 5, 13, and 2 W m^{-2}, respectively, which correspond to 7, 12, and 1% of mean buoy LHF. Again we find a somewhat high temporal correlation of satellite and *in situ* turbulent fluxes (Table 2), which tends to decrease in the tropics. Remaining sampling issues show moderately strong RMS errors, i.e. ~30 W m^{-2} for MFUK and tropical moorings and 37 W m^{-2} in the Atlantic western boundary sampled by NDBC moorings. The positive (buoy minus satellite) LHF biases at MFUK and NDBC locations are mainly related to the underestimation of high LHF (>200 W m^{-2}) at low q and/or for high winds. In fact, the satellite q is higher than *in situ* q in dry conditions (Figure 2) that leads to LHF underestimation. Excluding cases with buoy $q < 3$ g kg^{-1} reduces the satellite LHF biases down to 4 W m^{-2} (MFUK) and 6 W m^{-2} (NDBC) while the RMS error reduces to 25 W m^{-2} (MFUK) and 29 W m^{-2} (NDBC).

Satellite daily SHF has high correlation with *in situ* data at extratropical locations and somewhat reduced correlation in the tropics (Table 2). The biases at MFUK and NDBC moorings are lower than 2 W m^{-2} in magnitude, which are negligible. In the tropics where time mean SHF is weak, satellite SHF is overestimated by 4 W m^{-2}. This departure is related to the underestimation of air temperature in warm and humid conditions (not shown). These comparisons show improvements by the new satellite SHF. Indeed, the previous version of SHF (Bentamy et al. 2008) was biased by more than 10 W m^{-2} according to Santorelli et al. (2011).

For global comparisons, we select NOCS2.0 daily LHF and SHF with uncertainties lower than 40 and 20 W m^{-2}, respectively. The above thresholds are the median values of NOCS2.0 LHF and SHF errors. They are chosen in order to maintain sufficient *in situ* data for comparison. Consequently, most selected NOCS2.0 data are located in northern basins. The lowest NOCS2.0 data sampling is in the tropics and in southern latitudes. In particular, there is a factor of 20 between sampling lengths at 40° N and 40° S. The spatial distribution of the seasonal mean NOCS2.0 minus satellite LHF does not show any systematic basin-scale patterns. The highest positive differences (NOCS2.0 – satellite > 30 W m^{-2}) are found in the Mediterranean Sea throughout the year, and in western boundaries during local winter. To summarize, Figures 5 and 6 show NOCS2.0 and satellite LHF comparisons of zonally averaged fluxes stratified by ocean basin. The two LHF products have similar latitudinal dependencies, especially to the north, where *in situ* data coverage is better. For both data sets the zonal mean LHF exceeds 100 W m^{-2} in the trade wind zones (Figures 5

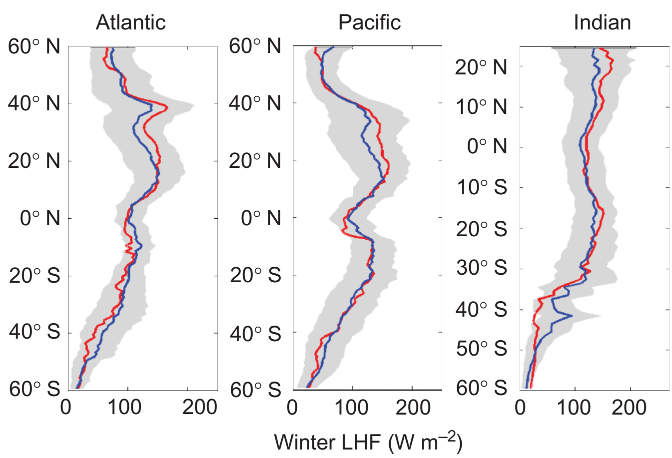

Figure 5. Latitudinal averages of NOCS2.0 (red) and satellite (blue) of LHF estimated over the Atlantic (left), the Pacific (middle), and the Indian (right) oceans for 2005–2007 boreal winter.

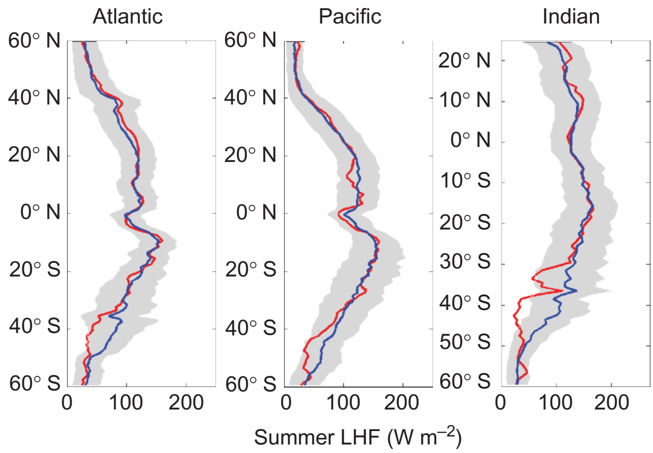

Figure 6. Latitudinal averages of NOCS2.0 (red) and satellite (blue) of LHF estimated over the Atlantic (left), the Pacific (middle), and the Indian (right) oceans for 2005–2007 boreal summer.

and 6), where rather strong winds and dry air are both present. Seasonal variability, which is pronounced in the Atlantic and Pacific, is associated with stronger winds in local winter. Both NOCS2.0 and satellite LHF indicate maxima along 40 and 36° N in the Atlantic and Pacific, respectively, during the winter season (Figure 5), reflecting contributions from high LHF in the western boundaries associated with winter storms. These high LHF are absent in local summer (Figure 6). Locally weak LHF is present throughout the year along the equator in the Atlantic and Pacific due to lower winds and rather cold SST in the eastern cold tongue regions. The lowest LHF is found at high latitudes due to cold SST and related low air humidity. Owing to sampling issues, discrepancies between NOCS2.0 and satellite LHF are stronger in southern oceans. For instance, near 40° S in the Atlantic and Indian Oceans, these exceed 30 W m^{-2} in boreal summer (Figure 6). Lower ship-based LHF may be linked to the need for ships to avoid stormy seas. Indeed, 90% of NOCS2.0 daily LHF along 40° S in the Indian Ocean are lower than 50 W m^{-2}, but this percentage is only 20% for satellite daily LHF.

Zonally averaged sensible heat fluxes from NOCS2.0 and satellite exhibit qualitatively similar behaviour (Figures 7 and 8). Both SHF estimates do not exceed 20 W m^{-2} in the tropics, and increase towards the mid-latitudes of the winter hemisphere. The highest sensible heat loss occurs around 40° N in the Atlantic and Pacific in boreal winter due to high winds and strong air–sea temperature difference (ΔT) in the western boundary regions. The northern SHF amplification is not present in local summer, reflecting a significant seasonal drop in storm track activity. Although the two SHFs are highly correlated, satellite SHF is higher than NOCS2.0. The difference is apparent during local winter, when it increases up to 25 W m^{-2} in the north Pacific between 30 and 40° N (Figure 7). Even higher differences occur in the southern ocean in austral winter (Figure 8). Discrepancies between NOCS2.0 and satellite SHF are more pronounced during the summer season in regions located south of 40° S, where satellite SHF exhibits much more seasonal variation than that of NOCS2.0. Summertime departures found at high southern latitudes are mainly associated with differences in wind speeds and with poor temporal and spatial samplings of NOCS2.0 daily data and missing strong wind events, which are avoided by ships.

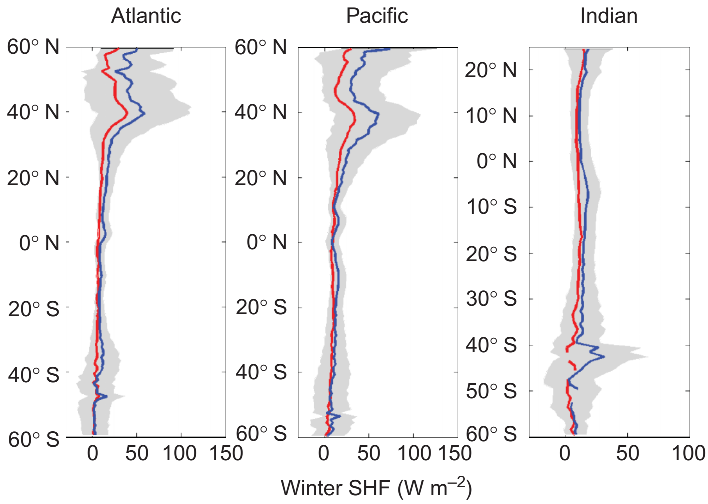

Figure 7. Boreal winter (DJF) zonal mean NOCS2.0 (red) satellite (blue) SHF over the Atlantic (left), Pacific (middle), and Indian (right) oceans for 2005–2007.

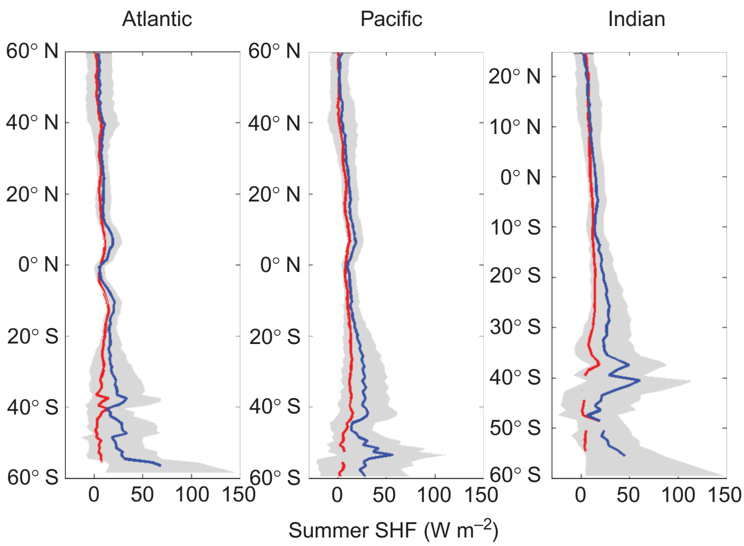

Figure 8. Boreal summer (JJA) zonal mean NOCS2.0 (red) satellite (blue) SHF over the Atlantic (left), Pacific (middle), and Indian (right) oceans for 2005–2007.

6. Conclusion

The presence of biases in the Bentamy et al. (2003) version of the IFREMER turbulent fluxes required improvement of the product. The availability of the new air–sea interaction gridded data set (NOCS2.0) calculated from height-adjusted ICOADS data allows for enhancement of satellite-derived, turbulent fluxes over the global ocean. The new version of the IFREMER satellite, turbulent air–sea fluxes is based on a synergy of remote-sensing and atmospheric reanalysis data. It includes a newly improved air humidity retrieval scheme, new QuikSCATV3 scatterometer winds, and adopts *t* from the ECMWF Era-Interim atmospheric reanalysis.

The core of the air humidity retrieval scheme remains unchanged. This is based on the statistical relationship between microwave brightness temperature and q_{10}, which in turn is based on the quasi-linear relationship between q_{10} and integral atmospheric water vapour content (Schultz et al. 1993). However, the direct application of this retrieval algorithm in Bentamy et al. (2003) results in a SST-dependent q_{10} bias, which suggests the inclusion of SST as an additional parameter in the satellite q_{10} retrieval algorithm. Furthermore, the analysis of q_{10} bias reveals a dependence on atmospheric stratification that reflects modifications in the relationship between water vapour content and q_{10} over ocean SST fronts. Therefore, the new q_{10} retrieval algorithm developed in this article includes SST and the air–sea temperature difference terms along with the traditional microwave brightness terms. The retrieval algorithm parameters are fitted using the global *in situ* data from the bias-corrected version of ICOADS (NOCS2.0). The new satellite q_{10} has a reduced bias that no longer depicts the large-scale patterns (dry tropics and wet subtropics) found in the previous IFREMER product.

All satellite observations are objectively mapped on a daily $0.25° \times 0.25°$ grid following Bentamy and Croizé-Fillon (2011). The validation of daily gridded q_{10} shows good comparisons with *in situ*, daily mean mooring measurements in the North Atlantic and tropics. The RMS values are about 1 g kg^{-1}, while the correlation coefficients exceed 0.85. Similar results are obtained from comparisons with daily NOCS2.0 data not used in the development of the satellite retrieval model.

Daily satellite LHF is slightly underestimated in comparison with *in situ* buoy data. The LHF bias (buoy minus satellite) is 5 W m^{-2} (or 7% of the mean buoy LHF) and 13 W m^{-2} (12%) at mid-latitudes locations (MFUK and NDBC moorings, respectively). It decreases to 2 W m^{-2} (1%) at the tropical moorings. SHF is slightly overestimated by 2 W m^{-2} (11%) at MFUK, by 2 W m^{-2} (7%) at NDBC, and by 4 W m^{-2} (51%) at the tropical moorings. On a global scale, satellite-derived LHF and SHF exhibit similar spatial and temporal patterns to those derived from NOCS2.0. Global comparisons between NOCS2.0 and satellite suggest that both LHF and SHF exceed *in situ* values for storm track belts during local winter, which are particularly evident at high southern latitudes. The increased difference in the south is in part explained by the poor temporal and spatial samplings of NOCS2.0 daily data and missing strong wind events, which are avoided by ships. Indeed, 90% of NOCS2.0 daily LHF along 40° S in the Indian Ocean is lower than 50 W m^{-2}, but this percentage is only 20% for satellite daily LHF.

Statistical comparisons between *in situ* (moorings and NOCS2.0) and satellite bulk variables and turbulent fluxes assess the improvement of the new calculations with regard to previous IFREMER satellite flux accuracy. In future, flux calculations will first be performed for the whole QuikSCAT period (August 1999–November 2009). The spatial and temporal patterns of the resulting flux fields will be investigated and compared with those derived from satellite observations such as HOAPS, from blended data such as AOFLUX, or from meteorological reanalyses such as ERA-Interim. The extension of the calculation to the periods of the European Satellite Remote Sensing satellites ERS-1 and ERS-2 (March 1992–January 2001) and of ASCAT (February 2007–present) is expected.

Acknowledgements

This research was supported by TOSCA (Terre, Océan, Surfaces continentales, Atmosphère) and SIMED (Simulation de la Mediterranée) projects, NFS (ATM0631685), and NASA (NNXIOAD99G, NNX09AF34G). We thank D. Crozé-fillon, F. Paul, J. F. Piollé, A. Santorelli, F. Kelly, and IFREMER/CERSAT for data processing support. The authors are grateful to ECMWF, EUMETSAT, CERSAT, JPL, NOAA, NOCS, Météo-France, NDBC, PMEL, and UK MetOffice for providing numerical, satellite, and *in situ* data.

References

Andersson, A., K. Fennig, C. Klepp, S. Bakan, H. Graßl, and J. Schulz. 2010. "The Hamburg Ocean Atmosphere Parameters and Fluxes from Satellite Data – HOAPS-3." *Earth System Science Data* 2: 215–234. doi:10.5194/essd-2-215-2010.1.

Ayina, L. H., A. Bentamy, A. Mestas-Nunez, and G. Madec. 2006. "The Impact of Satellite Winds and Latent Heat Fluxes in a Numerical Simulation of the Tropical Pacific Ocean." *Journal of Climate* 19: 5889–5902. http://dx.doi.org/10.1175/JCLI3939.1.

Bentamy, A., L.-H. Ayina, W. Drennan, K. Katsaros, A. Mestas-nuñez, and R. T. Pinker, 2008. "15 Years of Ocean Surface Momentum and Heat Fluxes from Remotely Sensed Observations." *FLUXNEWS*, No. 5, January 2008, World Climate Research Program, Geneva, 14–16. http://www.sail.msk.ru/newsletter/fluxnews_5_final.pdf

Bentamy, A., and D. CroizéFillon. 2011. "Gridded Surface Wind Fields From Metop/ASCAT Measurements." *International Journal of Remote Sensing* 33: 1729–1754.

Bentamy, A., S. A. Grodsky, J. A. Carton, D. Croizé-Fillon, and B. Chapron. 2012. "Matching ASCAT and QuikSCAT Winds." *Journal Geophysical Research* 117: C2. doi:10.1029/2011JC007479.

Bentamy, A., K. Katsaros, A. Mestas-Nuñez, W. Drennan, E. Ford, and H. Roquet. 2003. "Satellite Estimates of Wind Speed and Latent Heat Flux Over the Global Oceans." *Journal of Climate*16: 637–656. http://dx.doi.org/10.1175/15200442(2003)0160637:SEOWSA2.0.CO;2.

Bentamy, A., K. Katsaros, and P. Queffeulou. 2011. "Satellite Air Sea Fluxes." In *Remote Sensing of Changing Oceans*. http://www.springer.com/earth+sciences+and+geography/geophysics/book/978-3-642-16540-5.

Berry, D. I., and E. C. Kent. 2011. "Air-Sea Fluxes From NOCS2.0: The Construction of a New Gridded Dataset with Uncertainty Estimates." *International Journal Climatology* 31: 987–1001. CLIMAR-III Special Issue, doi:10.1002/joc.2059.

Bourras, D. 2006. "Comparison of Five Satellite-Derived Latent Heat Flux Products to Moored Buoy Data." *Journal of Climate* 19: 6291–6313. doi:10.1175/JCLI3977.1.

Chou, S.-H., E. Nelkin, J. Ardizzone, R. M. Atlas, and C.-L. Shie. 2003. "Surface Turbulent Heat and Momentum Fluxes Over Global Oceans Based on the Goddard Satellite Retrieval, Version 2 (GSSTF2)." *Journal of Climate* 16: 3256–3273.

Fairall, C. W., E. F. Bradley, J. E. Hare, A. A. Grachev, and J. B. Edson. 2003. "Bulk Parameterization of Air-Sea Fluxes: Updates and Verification for the COARE3.0 Algorithm." *Journal of Climate* 16: 571–591.

Fore, A., B. Stiles, R. S. Dunbar, B. Williams, A. Chau, L. Ricciardulli, F. Wentz, T. Meissner, and E. Rodridguez. 2011. "Point-Wise Wind Retrieval and Ambiguity Removal Improvements for the QuikSCAT Climatological Data Set." International Ocean Vector Wind Science Team Meeting, Annapolis, MD, May 9–11. http://coaps.fsu.edu/scatterometry/meeting/past.php#2011.

Grodsky, S. A., A. Bentamy, J. A. Carton, and R. T. Pinker. 2009. "Intraseasonal Latent Heat Flux Based on Satellite Observations." *Journal of Climate* 22 (17): 4539–4556. http://dx.doi.org/10.1175/2009JCLI2901.1.

Jackson, D. L., G. A. Wick, and F. R. Robertson. 2009. "Improved Multisensor Approach to Satellite-Retrieved Near-Surface Specific Humidity Observations." *Journal of Geophysical Research* 114: D16303. doi:10.1029/2008JD011341.

JPL (Jet Propulsion Laboratory). 2006. "QuikSCAT science data product user's manual (version 2.0)." *Jet Propulsion Laboratory Publication* D-18053, Pasadena, CA, 84 p. http://podaac.jpl.nasa.gov/quikscat

Kent, E., S. D. Woodruff, and D. I. Berry. 2007. "Metadata from WMO Publication No. 47 and an Assessment of Voluntary Observing Ship Observation Heights in NOCS2.0." *Journal of Atmospheric and Oceanic Technology* 24: 214–234.

Kubota, M., and T. Hihara. 2008. "Retrieval of Surface Air Specific Humidity over the Ocean using AMSR-E Measurements." *Sensors* 8: 8016–8026. doi: 10.3390/s812801.

Kubota, M., N. Iwasaka, S. Kizu, M. Konda, and K. Kutsuwada. 2002. "Japanese Ocean Flux Data Sets with Use of Remote Sensing Observations (J-OFURO)." *Journal of Oceanography* 58: 213–225.

Meissner, T., D. K. Smith, and F. J. Wentz. 2001. "A 10-Year Intercomparison Between Collocated Special Sensor Microwave Imager Oceanic Surface Wind Speed Retrievals and Global Analyses." *Journal of Geophysical Research* 106 (C6): 11731–11742.

Mestas-Nuñez, A., A. Bentamy, and K. Kristina. 2006. "Seasonal and El Nino Variability in Weekly Satellite Evaporation Over the Global Ocean During 1996–98." *Journal of Climate* 19: 2025–2035. http://dx.doi.org/10.1175/JCLI3721.1.

Portabella, M., A. Stoffelen, W. Lin, A. Turiel, A. Verhoef, J. Verspeek, and J. Ballabrera-Poy. 2012. "Rain Effects on ASCAT-Retrieved Winds: Toward an Improved Quality Control IEEE." *Transactions on Geoscience and Remote Sensing* 50: 2495–2506. doi:10.1109/TGRS.2012.2185933.

Reynolds, R. W., T. M. Smith, C. Liu, D. B. Chelton, K. S. Casey, and M. G. Schlax. 2007. "Daily High-Resolution-Blended Analyses for Sea Surface Temperature." *Journal of Climate* 20: 5473–5496.

Ricciardulli, L., and F. Wentz. 2011. *Reprocessed QuikSCAT (V04) Wind Vectors with Ku-2011 Geophysical Model Function*. Remote Sensing Systems Technical Report 043011. http://www.ssmi.com/qscat/qscat_Ku2011_tech_report.pdf

Santorelli, A., R. T. Pinker, A. Bentamy, W. Drennan, K. Katsaros, J. Carton, and A. Mestas-Nunez. 2011. "Differences Between Two Estimates of Air Sea Turbulent Heat Fluxes over the Atlantic Ocean." *Journal of Geophysical. Research* 116: No. C09028. doi: 10.1029/2010JC006927.

Schulz, J., P. Schlussel, and H. Grassl. 1993. "Water Vapour in the Atmosphere Boundary Layer over Oceans from SSM/I Measurements." *International Journal of Remote Sensing* 14: 2773–2789.

Simmons, A., S. Uppala, D. Dee, and S. Kobayashi.2006. "ERA-Interim: New ECMWF Reanalysis Products From1989 Onwards." *ECMWF Newsletter* 110: 26–35.

Tomita, H., and M. Kubota. 2006. "An Analysis of the Accuracy of Japanese Ocean Flux Data Sets with Use of Remote Sensing Observations (J-OFURO) Satellite-Derived Latent Heat Flux Using Moored Buoy Data." *Journal of Geophysical Research* 111: C07007. doi: 10.1029/2005 JC003013.

Wackernagel, H. 1998. *Multivariate Geostatistics*, 291 p. Berlin: Springer.

Yu, L., R. A. Weller, and B. Sun. 2004. "Improving Latent and Sensible Heat Flux Estimates for the Atlantic Ocean (1988–1999) by a Synthesis Approach." *Journal of Climate* 17: 373–393.